Removal of methyl violet 2B dye from aqueous solution by adsorption onto raw and modified carobs (*Ceratonia siliqua* L.)
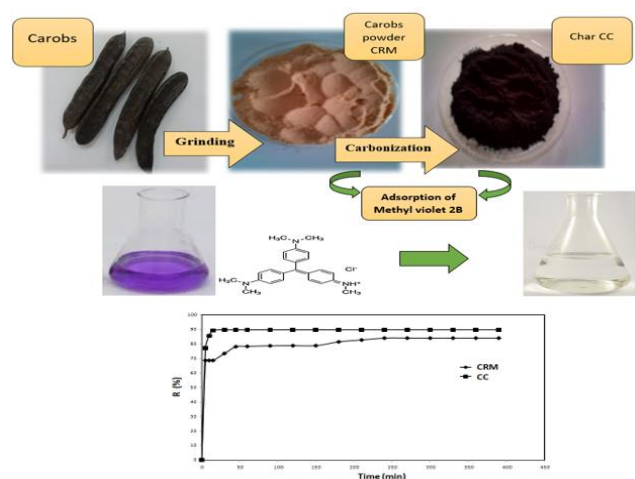
Kerzabi Y., Benomara A., and Merghache S.*

Laboratory of Inorganic Chemistry and Environment (LCIE), Department of Chemistry, Faculty of Sciences, University of Tlemcen, P.O. Box 119, Tlemcen 13000, Algeria
*to whom all correspondence should be addressed: e-mail: merghachesalima@yahoo.fr

Graphical abstract

Abstract

In the present study, fruits of *Ceratonia siliqua* L. (carobs) were used as an alternative low-cost biosorbents to remove a cationic dye, methyl violet 2B (MV) which has broad applications in paints, textile and printing ink, from aqueous solutions. The untreated (CRM) and thermal treated carobs (CC) were characterized by BET, FTIR, XRD and SEM techniques. The influences on MV adsorption of various experimental factors such as particle sizes, contact time, stirring speed, adsorbent dose, solution pH, temperature, ionic strength and initial MV concentration were investigated. Adsorption kinetics was found to be best represented by the pseudo second order model. The isotherm analysis indicated that the adsorption data could be represented by the Langmuir model for CRM and CC at 20°C. The maximum adsorption capacity for MV was 62.5 mg/g onto CC and 9.804 mg/g onto CRM. Thermodynamic parameters showed that the process was spontaneous and exothermic.

Keywords: *Ceratonia siliqua* L., methyl violet 2B, characterization, adsorption, kinetics, isotherms, thermodynamics.

1. Introduction

Industries, such as textile, leather, paper, plastics, cosmetics and others, use dyes in their process, which generates a considerable amount of colored wastewater. Over 100,000 dyes are commercially available. In addition, around 700,000 tons of dyes are produced annually and 10% of this quantity is discharged in effluent from textile and associated industries (Ramírez – Montoya *et al.*, 2014). Industrial wastewater containing such dyes, once released into the aquatic environment can contaminate surface water bodies and groundwater, which leads to serious damage to aquatic flora and fauna because the dyes can be toxic and mutagenic. The damage can be extended to the soil by leaching and irrigation (Xu *et al.*, 2011; Kabra *et al.* 2012). Therefore, removal of dyes from the effluents is very important for both aquatic ecosystem and human health.

Various techniques such as chemical coagulation, precipitation, ozonation, adsorption, oxidation, ion exchange, and photo degradation have been used for the removal of dyes from wastewaters (Jaikumar *et al.*, 2009). Biosorption is a preferred method due to the usage of low-cost materials, low energy usage, and high efficiency (Duan *et al.*, 2012). Material that can be regenerated and reused is considered as an added advantage. In biosorption process, dye molecule is adsorbed onto the biomass through physical or chemical adsorption and thus avoids the formation of degraded dye products which may be more harmful than the dye itself. Biosorption via "renewable biomass" is a key advantage over nonrenewable adsorbents such as clay, peat, zeolite, lignite, and some forms of activated carbons (Gallagher *et al.*, 1997).

Methyl violet 2B (MV), a basic dye that belongs to triphenylmethane class, is a dark green solid and dissolves in water to give an intense violet color. The structure of MV is shown in Figure 1. The dye has broad applications in paints, textile and printing ink. It is an active ingredient in biological stain and can also be used as a moderate class disinfectant. However, MV is revealed to be toxic as it can cause severe skin, respiratory, gastrointestinal tract and

---

Kerzabi Y., Benomara A., and Merghache S. (2022), Removal of methyl violet 2B dye from aqueous solution by adsorption onto raw and modified carobs (*Ceratonia siliqua* L.), *Global NEST Journal*, **24**(4), 706-719.

eye irritations (Sabnis *et al.*, 2010). Due to its intense color, even a small amount of MV in water would produce a noticeable coloration. For these reasons, it is imperative to have an effective method to remove MV from industrial wastewater before being discharged into the environment.

Low-cost materials such as dragon fruit skin (Ahmad *et al.*, 2021), peat (Guillén *et al.*, 2022), pinewood (Yu *et al.*, 2020), banana peel (Ramutshatsha – Makhwedzha *et al.*, 2022), orange peel (Akinhanmi *et al.*, 2020) and fly ash (Behrami et al, 2022), have been researched for their ability as biosorbents. *Ceratonia siliqua* tree is native to the Mediterranean region including Southern Europe, Northern Africa, the larger Mediterranean Islands, the Levant and Middle East of Western Asia into Iran; and the Canary Islands and Macaronesia (GRIN, 2017)**.** Studies on the removal of some dyes: Methylene blue (Gezer, 2018; Bounaas *et al.*, 2021)**,** reactive black 5 (Güzel *et al.*, 2015), basic green 4 and direct red 28 (Saygılı *et al.*, 2018) and some heavy metals such as Zn(II), Ni(II), Cu(II), Cd(II), Co(II), Cr (VI) and Pb (II) ions (Farhan *et al.*, 2012; Farnane *et al.*, 2017; Bouaouina *et al.*, 2022; Deniz Çiftçi *et al.*, 2020) from aqueous solutions, had been done using carob, the fruit of *Ceratonia siliqua* as biosorbent. According to our literature knowledge, there is no information related to the utilization of carob which is very abundant and inexpensive material in Mediterranean countries, as biosorbent for removing the Methyl violet 2B dye. Therefore, this study aims to explore the potential of untreated (CRM) and thermal treated carobs (CC) as biosorbents for the removal of methyl violet 2B (MV) dye in an aqueous solution. The adsorbents characteristics and the effects of different parameters such as particle sizes, contact time, stirring speed, adsorbent dose, solution pH, temperature, ionic strength and initial dye concentration were investigated. The adsorption kinetic models, isotherm models, and thermodynamic parameters were also studied.
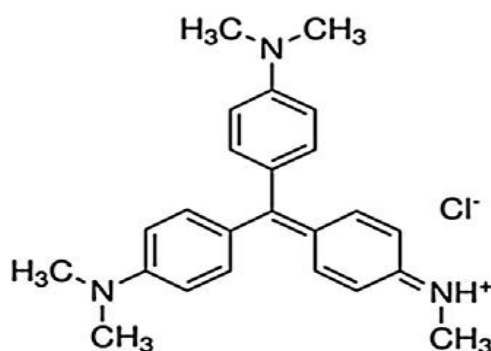

Figure 1. Chemical structure of MV molecule.

2. Materials and methods

2.1. Adsorbent material

Ceratonia siliqua fruits (carobs) were collected from Lourit–Tlemcen situated in the west of the north of Algeria. *C. siliqua* fruits were thoroughly rinsed with distilled water to remove dust and then they were allowed to dry at room temperature. The dried material was crushed and grounded into a fine powder in two grinding mills (LAFERTET and RESTSCH). The powder was then sieved to get several fractions using CONTROLAB apparatus. The *C. siliqua* fruits powder (CRM) was dried in an oven at 50 ℃ and then stored in a desiccator to be used for the batch experiments. The *C. siliqua* fruits powder (CRM) was used as raw material to produce the char by heat treatment (carbonization). Experiments were carried out in a Muffle Furnace (GALLENKAMP). The powder was then heated slowly to reach desired temperature of 450 °C. It was kept under this temperature for 1 hour, and then cooled down to room temperature. The char obtained (CC) was then stored in a desiccator for later experimental use.

2.2. Adsorbate material

Methyl violet 2B which is the most commonly used material for dying cotton, wood, and silk is a heterocyclic aromatic chemical compound with ($C_{24}H_{28}N_3Cl$) as molecular formula and a molecular weight of 393.96 g /mol (Dahri et al, 2016; Cengiz at al., 2010). Methyl violet 2B was purchased from Fluka AG, chemische fabrik. A stock solution of 1000 mg/L of methyl violet 2B (MV) was prepared for calibration purposes. From the stock, different concentrations of MV were prepared by diluting with distilled water. The calibration curve was plotted from the dye solution prepared in the concentration range of 0.1 to 10 mg/L. MV dye in the aqueous solution was analyzed using JENWAY 7300 UV – VIS spectrophotometer at 580 nm.

2.3. Characterization of adsorbent material

2.3.1. The textural properties

The measurement of the specific surface of pore, diameters and pore volume of CRM and CC were obtained by using the nitrogen adsorption – desorption isotherm curve at -196°C (Micromeritics ASAP 2020 MP apparatus) using the Brunauer – Emmett – Teller (BET) and Barrett – Joyner – Halenda (BJH) methods. Prior to the measurements, the apparatus was outgassed at 320 °C under nitrogen flow for 5 h. The BET surface area, pore volume and pore size of the prepared adsorbents were then determined.

2.3.2. FTIR analysis

Functional groups on adsorbent's surface were identified using Fourier transform infrared (FTIR) (Perkin Elmer spectrophotometer) in the scanning range of 4000 – 450 cm^{-1}. Spectroscopy grade KBr was dried in an oven at 110 °C before use. Samples (0.002 g) were grinded with KBr (0.15 g) using mortar and pestle.

2.3.3. XRD analysis

To analyze crystalline nature of the adsorbents, XRD studies were carried out on an X–ray powder diffractometer Rigaku MiniFlex 600 at 40 kV and 15 mA with CuKα radiation.

2.3.4. SEM analysis

Surface morphology analysis of adsorbents was carried out by using a HITACHI TM – 1000 Scanning Electron Microscope (SEM), with an accelerating voltage of 15 kV.

2.4. Batch adsorption studies

Batch experiments were carried out by mixing 75 mL of known concentration of MV solution (10 mg/L) with 0.25 g of adsorbent in a 250 mL conical flask. The mixtures were then agitated for 180 min on a magnetic stirrer at 500 rpm. The tests are carried out at room temperature (≈22° C) and at pH of the solution (pH ≈ 6.5). Various studies such as effect of particle size of adsorbent CRM (≤ 0.08 – 0.315 mm), effect of contact time (1 – 390 min), effect of agitation speed (100 – 1000 rpm), effect of adsorbent dose (0.01 – 1.5 g), effect of medium pH (3 – 11), effect of temperature (10 – 50 °C) and ionic strength (0 – 1.0 mol/L) were done for optimizing the experimental conditions. The effect of initial dye concentration (10 – 80 mg/L) was investigated using the optimal parameters. The medium pH was adjusted using aqueous solutions of HCl and NaOH 1M. After each adsorption process, the samples were centrifuged (5000 rpm, 10 min) for solid – liquid separation and the residual dye concentration in solution was analyzed by a UV–Vis spectrophotometer (JENWAY 7300) at 580 nm wave length.

The removal percentage (R, %), the amount of MV2B adsorbed at time t (q_t, mg/g), and the adsorption capacity at equilibrium (q_e, mg/g) were calculated by applying equations (1), (2) and (3), respectively:

$$R\,(\%) = \frac{C_0 - C_t}{C_0} \times 100 \qquad (1)$$

$$q_t = \frac{(C_0 - C_t)}{m} \times V \qquad (2)$$

$$q_e = \frac{(C_0 - C_e)}{m} \times V \qquad (3)$$

Where C_0 is the initial dye concentration (mg/L), C_e is the equilibrium dye concentration (mg/L), C_t is the dye concentration at the time t (mg/L), V is the volume of MV solution used (L) and m is the mass of adsorbent used (g).

3. Results and discussion

3.1. Characterization of CRM and CC

3.1.1. The textural properties of CRM and CC

The surface area, pore volume and pore size of particles were determined by BET and BJH methods and the values are presented in Table 1. BET and BJH surface areas of CRM are 1.992 and 7.215 m^2/g respectively. On the other hand, for CC, the BET and BJH surface areas are 115.667 and 88.421 m^2 /g respectively. The BJH pore sizes of CRM and CC are 118.387 and 13.66 nm respectively, which indicates the porous structure of CRM and CC which aids in MV adsorption (Tanada et al, 1980). From the data, it is evident that the BET surface area and pore volume of CC were greatly improved, indicating pore development during the carbonization stage.

3.1.2. FTIR analysis of CRM and CC

FTIR spectra before and after MV adsorption of CRM and CC are represented in Figures 2 and 3. Figure 2 shows the spectrum of CRM which contains a number of peaks reflecting its complex nature. The spectrum of native CRM shows the strong absorption band around 3390 cm^{-1} due to the vibrations stretching of the O − H bond and suggests the presence of hydroxyl (− OH) groups in the cellulose, lignin and water molecules. This band shifted to 3430 cm^{-1} after MV adsorption, indicating that − OH groups play an important role in the adsorption of MV.
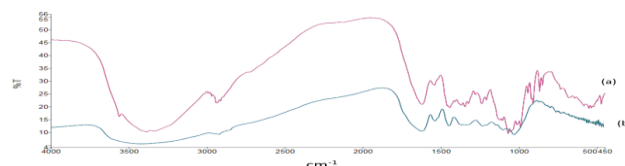

Figure 2. FTIR Spectrums of CRM before adsorption of MV (a), after adsorption of MV (b).

The band at 2943 cm^{-1} is due to the C − H stretching vibrations which has become less finer after adsorption at 2919 cm^{-1}. The stretching vibrations of methoxy group (CH$_3$ − O), before adsorption, was observed around 2871 cm^{-1}, which shifted to 2870 cm^{-1} after adsorption. The band of 1619 cm^{-1} before adsorption, is attributed to the bending vibration C = C. This band shifted to 1624 cm^{-1} after adsorption. The bands observed at 1444 cm^{-1} and 1450 cm^{-1}, before and after adsorption respectively, are due to the skeletal C = C vibration in aromatic rings on the surface of the adsorbent. The band at 1069 cm^{-1} before adsorption is assigned to O − H bands and C − OH stretching of phenolic groups. The strong band of C − O at 1024 cm^{-1} before adsorption and at 1030 cm^{-1} after adsorption, confirms the lignin and cellulose structures of *C. siliqua* fruits. In addition, the peak at 868 cm^{-1} of the material indicated the presence of C − H derivatives in the aromatic rings, which has disappeared after adsorption. The observed shifts in these functional group's stretching bands suggest that adsorption of MV onto CRM's surface involves these functional groups. New bands appeared such as the peak at 1538 cm^{-1}, which may be occurring from the interactions between the adsorbent surface and dye molecules. In addition, we also notice the disappearance of certain bands (1069, 868 cm^{-1}) confirming the adsorption of the dye (Auta *et al.*, 2013; Farnane *et al.*, 2012; Güzel *et al.*, 2015; Farnane *et al.*, 2017). FTIR spectra of CC before and after adsorption of MV are shown in Figure 3. In the spectra of CC before adsorption (Figure 3(a)), the broad band around 3421 cm^{-1} represents the O − H stretching vibrations. The band observed at 2936 cm^{-1} indicates the presence of C − H stretching vibrations. The band stretching at 1036 cm^{-1} indicates the presence of C − O. From FTIR spectrum (Figure 3(b)), after adsorption of MV, shifts can be observed in these functional groups' stretching bands. This suggests that adsorption of MV onto CC's surface involves these functional groups. Additionally, new bands appeared between 474 – 628 cm^{-1}, these bands may be occurring from the interactions between the adsorbent surface and dye molecules. The comparison between the

FTIR spectra of CRM (Figure 2(a)) and its carbonized product CC (Figure 3(a)) before adsorption, shows the disappearance of the majority of the bands because when the raw carob was heated at 450 °C for 1 h, certain the functional groups were dramatically destroyed.

Carbonization resulted in significant changes in the surface functional groups of adsorbents. The changes also include a decrease in intensity of bands, shifting of bands, and loss of the bands. This is in agreement with the works of Daramy (Daramy *et al.*, 2020).

Table 1. The textural characteristics of CRM and CC obtained from N_2 adsorption – desorption analysis.

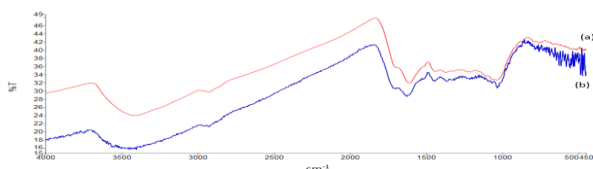| Properties	CRM	CC
BET surface area (m^2/g)	1,992	115,667
BJH Adsorption cumulative surface area of pores (m^2/g)	7,215	88,421
BJH Adsorption cumulative volume of pores (cm^3/g)	0,214	0,302
BJH Adsorption average pore width (nm)	118,387	13,660

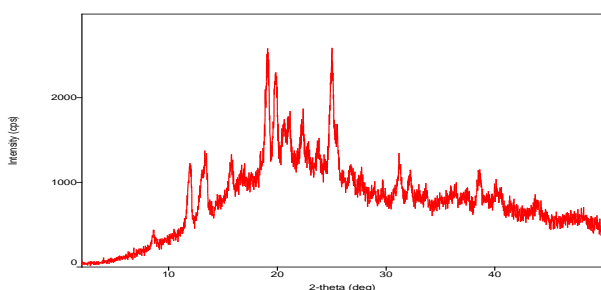**Figure 3.** FTIR Spectrums of CC before adsorption of MV (a), after adsorption of MV (b).
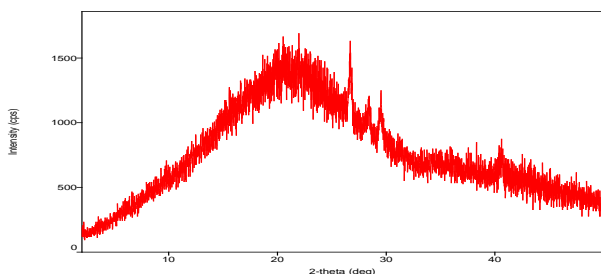

Figure 4. XRD patterns of CRM.

Figure 5. XRD patterns of CC.

3.1.3. Crystal structure analysis of CRM and CC

XRD pattern was studied in 2Ө range 0 – 50°. The X – ray diffraction profiles for CRM and CC are shown in Figures 4 and 5 which display the small angle XRD of CRM and CC. There is a significant difference between CRM and CC profiles. The XRD pattern of CRM (Figure 4) shows an amorphous structure of the material and also exhibits four characteristic peaks of cellulose at 2Ө: 15.81°, 2Ө: 20.99°, 2Ө: 24.94° and 2Ө: 31.25°. However, the XRD pattern of CC (Figure 5) shows broad diffraction peak situated at 2Ө: 10 – 30° and absence of intense peak that disclosed generally amorphous structure, which is favorable feature for well – defined adsorbents. This indicated that

crystalline nature was changed after carob transformed to char (Güzel *et al.*, 2015; Ciolacu *et al.*, 2011).

3.1.4. Surface morphology of CRM and CC

Scanning electron microscopy (SEM) has been a primary tool for characterizing the surface morphology and fundamental physical properties of the adsorbent. SEM micrographs of CRM and CC before and after adsorption of MV are shown in Figures 6 and 7 respectively. Figure 6(a) illustrates the SEM image for surface morphology and the approximate size of the raw carob before adsorption of MV. The carob particles appear distributed homogeneously with irregular shape. The external surfaces of this material show rough surface morphology, aggregates and reliefs of particles, large cavities which are very irregular. These cavities can behave like macropores. These increase the active sites which will increase the number of molecules adsorbed on the material surface (Hema *et al.*, 2009). Adsorption of MV onto CRM shows that the surface has changed (Figure 6(b)). The adsorbent is plated by dye molecules along the surface. The MV dye molecules appear to have created a film masking the voids in certain cavities, between the aggregates and the reliefs of the particles, and MV is clearly seen to be adsorbed onto the surface (Kismir *et al.*, 2011). SEM photographs of the biosorbents shown in Figures 6(a) and 7(a), indicate significant differences between the surface morphology of CRM and CC. It could be seen that, after the treatment process, new wide pores are formed due to the carbonization of raw material. Pore walls got opened with many different sizes and shapes cavities. Traditionally, chars have been prepared from a number of carbon – rich biomasses such as raw materials using thermal process like carbonization. During this process, organic matter is burned leading to the formation of a high level of carbon and creating structures with well – defined pore size distributions (Haber *et al.*, 2002). The porosity of CC could be the reason of the large adsorption capacity of MV which is clearly seen by the change in the surface morphology of this adsorbent. The micrograph presented in Figure 7(b) shows clearly the dye-loaded adsorbent, coated by dye molecules over the whole surface. The dye molecules seem to have formed a void-free film masking the reliefs of particles and porosity of the aggregates (Kismir *et al.*, 2011).

3.2. Preliminary adsorption studies

Preliminary adsorption experiments were conducted to determine the optimal conditions for the removal of MV by the carob power CRM and the char CC regarding the particle size, contact time, agitation speed, adsorbent dose, initial pH, temperature, ionic strength and the initial dye concentration.
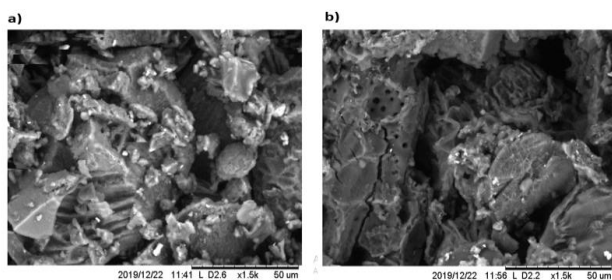

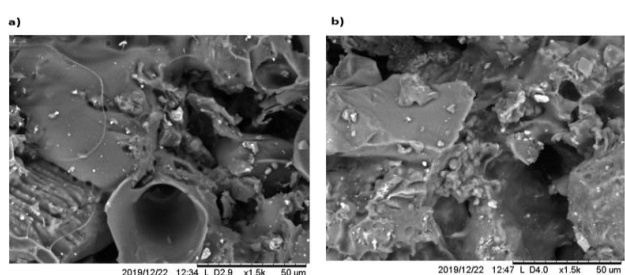**Figure 6**. SEM micrographs of CRM before (a) and after MV adsorption (b).

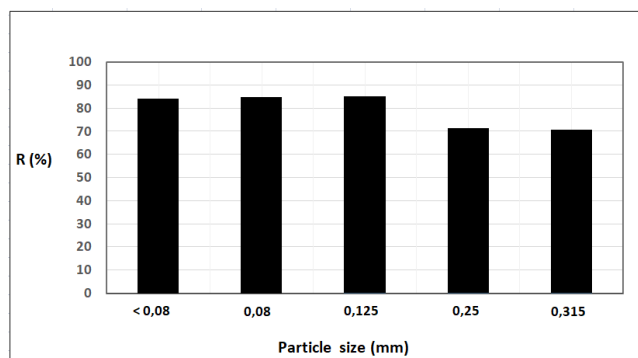**Figure 7.** SEM micrographs of CC before (a) and after MV adsorption (b).

Figure 8. Effect of the particle size on the adsorption of MV dye onto CRM.

3.2.1. Effect of particle size

Particle size of an adsorbent played a very important role in the adsorption capacity of dye. MV dye adsorption was investigated for different particle sizes (≤0.08 – 0.315 mm) of carob powder. The effect of these particle sizes on the percentage of dye adsorption R (%) is shown in Figure 8. It can be seen that CRM with particle sizes 0.25 mm and 0.315 mm shows relatively low removal percentage 71.3 and 70.5 %, respectively. CRM with particle size ≤ 0.08 and 0.125 mm shows a higher removal percentage (84.1 – 85%). Generally, the smaller particles will increase the dye adsorption of a given mass of adsorbent. This arises for the following reasons (Treybal *et al.*, 1981).

- smaller particles have a greater external surface area available for adsorption than larger particles.

- smaller particles move faster in solution than larger particles

- the boundary layer on adsorbent particles becomes relatively thin as a result of the high shear force at the particle surface and hence the external mass – transfer coefficient will increase as the mean particle diameter decreases.

Therefore, all experiments in the study were carried out by using CRM particle size ≤ 0.08 − 0.125mm based on the experimental results.

3.2.2. Effect of contact time

Equilibrium time is one of the most important parameters in the design of economical of wastewater treatment systems. Figure 9 represents the adsorption percentage of MV versus contact time for CRM and CC, at concentration equal to 10 mg/L. The adsorption is initially fast, and then slowing. The equilibrium was attained in about 240 and 15 min with removal percentage 84% and 89.9% for CRM and CC respectively. The adsorption of MV onto CC is a rapid process. The fast adsorption at the initial stage was probably due to the great concentration gradient between the dye in solution and the dye onto the adsorbent because there must be a number of vacant sites available at the beginning. The progressive increase in adsorption and consequently, the attainment of equilibrium adsorption is initially due to the limited mass transfer of the dye molecules from the bulk solution to the external surface of the adsorbent and are subsequently due to the slower internal mass transfer within the adsorbent particles (Güzel *et al.*, 2015; Yao *et al.*, 2011). The elimination yields of MV by CC are greater than those obtained in the case of CRM. This is probably due to the fact that CC has a specific surface higher than that of CRM.
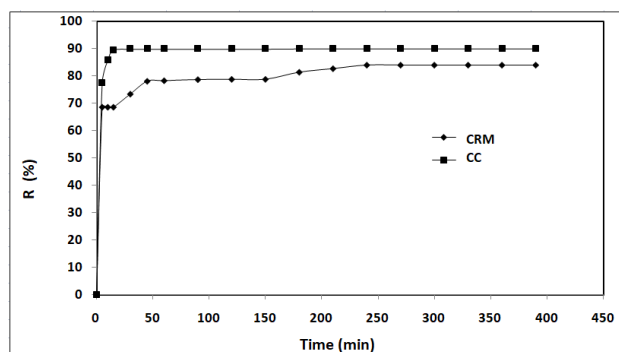

Figure 9. Effect of the contact time on the adsorption of MV dye onto CRM and CC.

3.2.3. Effect of agitation Speed

Agitation is an important parameter in adsorption phenomena influencing the distribution of the solute in the bulk solution and the formation of the external boundary film. Generally, the rate of dye adsorption is influenced by the degree of agitation and the uptake increases with agitation rate. The effect of adsorption of MV onto CRM and CC was studied at different agitation speeds. The results are shown in Figure 10. The optimum agitation speed for MV removal was found to be 500 rpm for CRM and 300 rpm for CC, with removal percentage

80.4% and 91% respectively. This is because at very slow agitation speed the adsorbent accumulates at the bottom, reducing the contact surface area of the adsorbent with the adsorbate. Moreover, at very high speed, centrifugal forces operate, resulting in desorption of the adsorbate (Salman *et al.*, 2012).
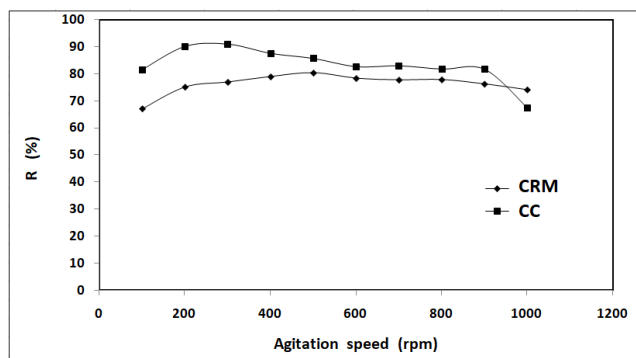

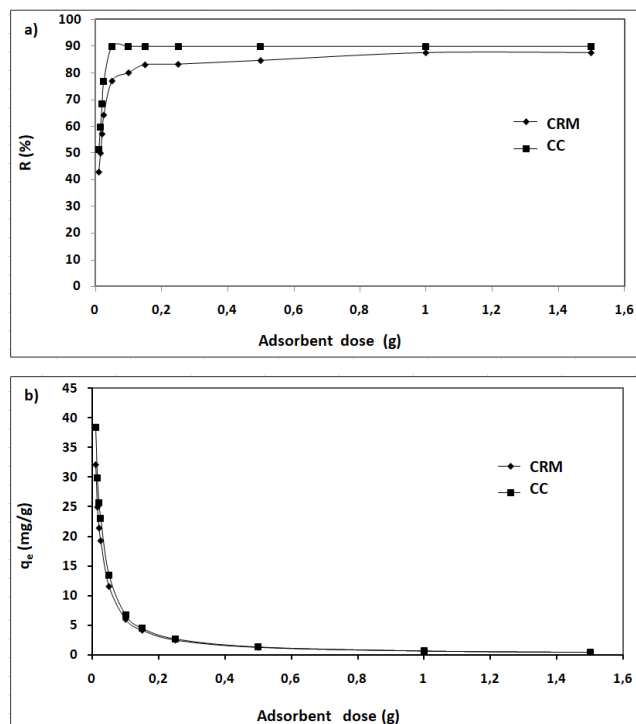**Figure 10**. Effect of the agitation speed on the adsorption of MV dye onto CRM and CC.

Figure 11. Effect of the adsorbent dose on the adsorption of MV dye onto CRM and CC.

3.2.4. Effect of adsorbent dose

The adsorbent dose is an important parameter in adsorption studies because it determines the capacity of adsorbent for a given concentration of dye solution. The effect of adsorbent dose on the dye removal percentage is shown in Figure 11. The experiments were carried out with adsorbent dose varied from 0.01 to 1.5 g with keeping other parameters constant. Figure 11(a) presents the percentage removal of MV from aqueous solution by CRM and CC at different adsorbent dosages. The percentage removal of MV increased from 42. 8% to 87.6% for CRM and 51.2% to 89.9% for CC as the CRM and CC dosages were increased from 0.01 to 1.5 g. The increase in percentage removal of the dye with increase in

adsorbent dose may be attributed to increased adsorption surface area and availability of more adsorption sites which increases with increase in adsorbent dose (Santhi *et al.*, 2009). As shown in Figure 11(b), the amount of MV adsorbed onto the CRM and CC was found to decrease from 32.1 to 0.44 mg/g and 38.4 to 0.45 mg/g respectively with increasing adsorbent dose. This may be due to two factors. First, the increase in adsorbent mass at fixed dye concentration and volume will lead to unsaturation of adsorption sites through the adsorption process, and second, the reduction in adsorbent capacity may be also due to particle aggregation, resulting from high adsorbent mass. Such aggregation would lead to a decrease in total surface area of the adsorbent and an increase in diffusional path length (Oladoja *et al.*, 2009). It is evident that the optimum dose for adsorption is 1 g for CRM and 0.05 g for CC, beyond these values a relatively constant adsorption performance was witnessed. The removal of MV dye by char CC was higher than by raw material CRM due to the carbonization of adsorbent that offered more pores to the surface of char than the untreated carobs.
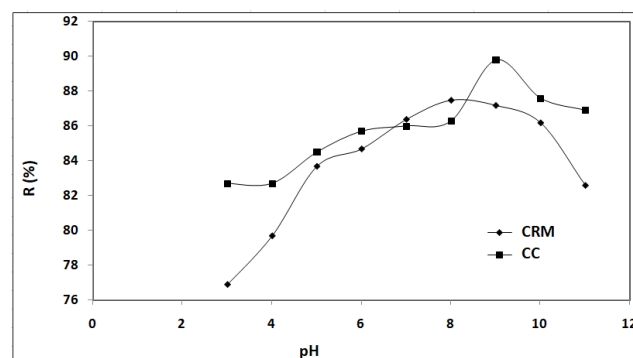

Figure 12. Effect of the initial pH on the adsorption of MV dye onto CRM and CC.

3.2.5. Effect of solution pH

The pH solution plays an important role in the whole adsorption process, particularly affecting the adsorption capacity of the adsorbent, the degree of ionization of the material present in the solution and the dissociation of the functional groups of the active sites of the adsorbent (Kim *et al.*, 2012). The hydrogen ion and hydroxyl ion are adsorbed quite easily, therefore the adsorption of other ions can be affected by the pH of the solution. It was necessary to discuss the effect of pH on the adsorption of MV. Thus, the effect of pH on MV removal has been studied by varying the pH over a range of 3 to 11 in order to determine the optimum pH value. The obtained data are shown in Figure 12. As shown in this figure, the pH significantly affected the adsorption percentage onto the two adsorbents CRM and CC. As initial solution pH increased from 3 to 8, the adsorption percentage onto CRM increased from 76.9% to 87.5%, after which there was a slight decrease in adsorption (R = 82.6% at pH = 11). The observed pH trend clearly indicates that the maximum adsorption of MV dye takes place at pH = 8. The percentage removal of MV onto CC, was also found to increase when the solution pH was increased from pH = 3 (R = 82.7%) to pH =9 (R= 89.8%). As pH increases from 9 to

11, adsorption efficiency decreased from 89.8% to 86.9%. The optimum adsorption was found at pH = 9. At lower values of pH. The surface of the adsorbent gathers positive charges by absorbing H^+ ions, which prevent the adsorption of dye ions onto adsorbent surface due to electrostatic repulsion and the competition between H^+ ions and MV for the adsorption sites (Kumar *et al.*, 2010). As the solution pH increased, the number of negatively charged surface sites on the adsorbent increased, which may result in the increase in adsorption of cationic dye molecules due to the electrostatic attraction (Amin *et al.*, 2009). The decrease in adsorption beyond pH=8 for CRM and pH =9 for CC is due to the formation of soluble hydroxy complexes between the adsorbent and the dye (Astuti *et al.*, 2017).

3.2.6. Effect of temperature

Temperature plays key role in adsorption process because it influences mobility and solubility of dye molecules in aqueous solution and surface properties of adsorbent. The study of the temperature effect on the adsorption process indicates whether the change is exothermic or endothermic one. The effect of the temperature was investigated at the concentration of MV solution equal to 10 mg/L. The temperature values are ranged in the present investigation from 10°C to 50°C.The results are shown in Figure 13. By increasing the temperature from 10 to 20°C, the percentage removal increased from 71.3% to 83.4% for CRM and from 82.5% to 87% for CC. Thus, the adsorption of MV is an endothermic process in nature.
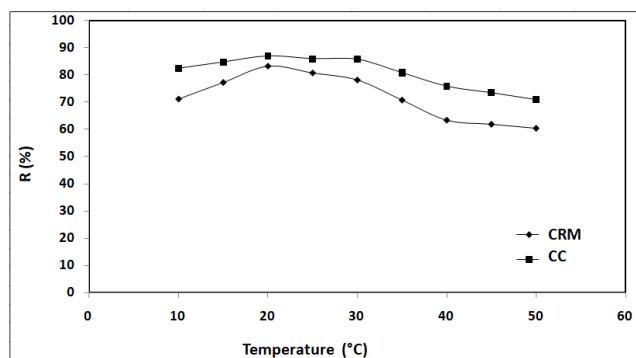

Figure 13. Effect of the temperature on the adsorption of MV dye onto CRM and CC.

This may be explained on the basis of the fact that increase in temperature enhances the rate of diffusion of the adsorbate molecules across the external boundary layer and in the internal pores of the adsorbent particles as a result of the reduced viscosity of the solution. In addition, the mobility of sorbate molecules also increases with temperature. However, an increase in the mobility of the dye molecules facilitates the dye molecules to move to the adsorbent surface, which causes an increase in the removal efficiency as the solution temperature increases. By increasing the temperature from 20°C to 50°C, the percentage removal decreased from 83.4% to 60.5% for CRM and from 87% to 71.1% for CC. This observation suggests that the adsorption of MV dye by CRM and CC in this temperature range is an exothermic process. This decrease in removal efficiency with increase in

temperature can be attributed to the weakening of the physical bonding between the adsorbate (MV dye molecules) and the active sites of the adsorbent which helps in detachment of dye molecules from the surface of adsorbent causing in reduced adsorption at elevated temperatures. The MV dye solubility also increased with increase in temperature resulting in the interaction between the solute and the solvent to be stronger than that between the solute and the adsorbent. Therefore, the adsorption of solute would be more difficult (Patil *et al.*, 2011).

3.2.7. Effect of ionic strength

The ionic strength of the solution is one of the factors that control both electrostatic and non – electrostatic interactions between the adsorbate and the adsorbent surface. The influence of ionic strength on the adsorption of MV onto CRM and CC was investigated using NaCl solutions of concentrations ranging from 0 to 1 mol/L, at constant dye concentration of 10 mg/L. The effect of ionic strength on the adsorption ability was demonstrated in Figure 14. As the ionic strength increased (C_{NaCl} varies between 0 and 1 mol/L), the adsorption percentage increased from 80.4% to 100% for CRM and from 84.5% to 92.5%. These results were similar to earlier findings by other workers for adsorption of MV onto stevensite rich clay (Elass *et al.*, 2001) and reactive blue 221 on kaolinite (Karaoğlu *et al.*, 2010). The higher adsorption percentage of methyl violet under these conditions especially in the case of CRM, can be attributed to the aggregation of MV cations induced by the action of salt ions, i.e., salt ions force dye molecules to aggregate, increasing the extent of adsorption onto CRM and CC surfaces. A number of intermolecular forces have been suggested to explain this aggregation, these forces include Van Der Waals forces; ion – dipole forces; and dipole – dipole forces, which occur between dye molecules in the solution. It has been reported that these forces increased upon the addition of salt to the dye solution (Eren *et al.*, 2010)**.**

Figure 14. Effect of the ionic strength on the adsorption of MV dye onto CRM and CC.

3.2.8. Effect of initial dye concentration

The initial dye concentration is one of the important factors that affect adsorption. The initial dye concentration of 5, 10, 20, 40, 60 and 80 mg/L were used in our study at 20 °C using the optimal values of agitation speed, adsorbent dose and initial pH. The results are presented in Figure 15. From this figure, it can be

observed that the adsorption capacity at equilibrium q_e increased with an increase in the initial MV concentrations. This is because as the initial concentration increases, the resistances against the mass transfer of the dye molecule from solution to the solid phase are overcome by the mass transfer driving force and hence more sorption occurs. Also, an increase in concentration results in an increase in the interaction between the dye molecule and adsorbents, therefore, increases the sorption process (Eren *et al.*, 2007). Adsorption capacity q_e of CC increased from 7.22 to 57.96 mg/g when initial concentration of MV increased from 5 to 80 mg/L. This trend appeared to be least significant in the case of CRM (q_e varies from 0.34 to 5.81 mg/g) which can be related to their least internal surface area (Table 1).
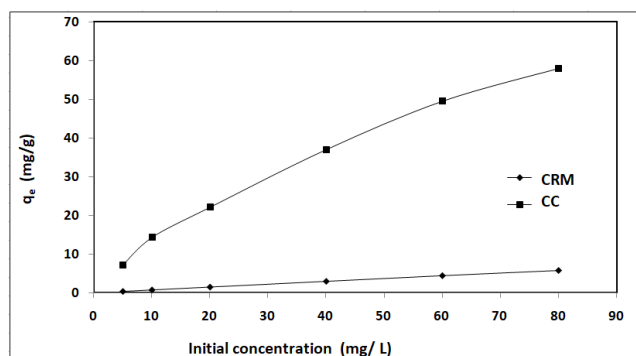

Figure 15. Effect of the initial dye concentration solution on the adsorption of MV dye onto CRM and CC.

3.3. Kinetic modeling

Adsorption kinetic defines the best model to describe experimental data. In this study, three kinetic models (the pseudo first order, pseudo second order and intraparticle diffusion) were used to fit the experimental data from the adsorption of MV dye onto carob powder CRM and char CC at initial dye concentration C_0 = 10 mg/L, at ambient temperature T ≈ 22°C and using agitation speed = 500 rpm, adsorbent dose = 0.25 g and initial pH ≈ 6.5. The conformity between the experimental data and the model predicted values was expressed by the correlation coefficients (R^2) and the comparison of the value of q_e calculated with that determined experimentally. For the pseudo first order model, a linear equation is obtained as follows (Lagergren *et al.*, 1898):

$$ln\left(q_e - q_t\right) = \ln q_e - k_1 t \tag{4}$$

Where q_e (mg/g) and q_t (mg/g) are the adsorption capacities at equilibrium and at time t, respectively, and k_1 (min^{-1}) is the rate constant. The pseudo first order rate constant k_1 values and adsorption capacity q_e were calculated from the slope and the intercept of the plots of $\ln(q_e - q_t)$ versus t.

The pseudo second order model is presented by following equation (Eba *et al.*, 2010)

$$\frac{t}{q_t} = \frac{1}{k_2 q_e^2} + \frac{1}{q_e} t \tag{5}$$

Where k_2 is the pseudo second order rate constant of adsorption *(g/mg.min)*. The q_e and k_2 values of the pseudo second order kinetic model can be determined from the slope and the intercept of the plots of $\dfrac{t}{q_t}$ versus t.

The pseudo first order and pseudo second order models cannot identify the diffusion mechanism and rate controlling steps that affect the adsorption process, thus intraparticle diffusion model based on the theory proposed by Weber and Morris (Weber *et al.*, 1963) was tested. According to this theory, the intraparticle diffusion equation is expressed as follows

$$q_t = K_d \, t^{1/2} + C \tag{6}$$

Where K_d (mg/g.min$^{1/2}$) is the intraparticle diffusion rate constant and C (mg/g) is a constant that gives an idea about the thickness of the boundary layer, where a value of C close to zero indicates that diffusion is the only controlling step of the adsorption process. If the mechanism of adsorption process follows the intra – particle diffusion, then the plot of q_t versus. $t^{1/2}$ would be a straight line and the K_d and C can be calculated from the slope and intercept of the plot, respectively. The results kinetic modeling is summarized in Figures 16–18.
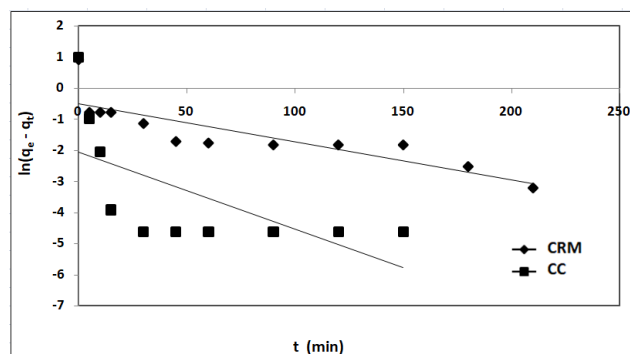

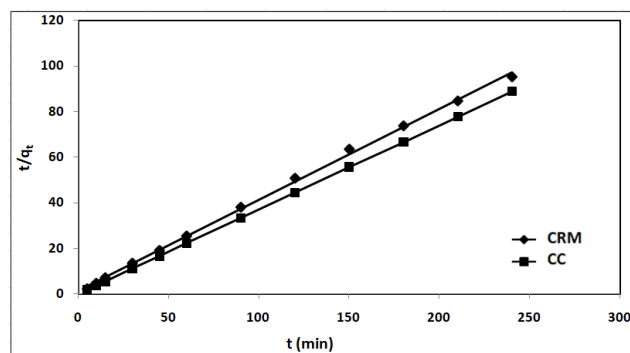**Figure 16.** The plots of pseudo first order kinetic model for MV adsorption onto CRM and CC.

Figure 17. The plots of pseudo second order kinetic model for MV adsorption onto CRM and CC.
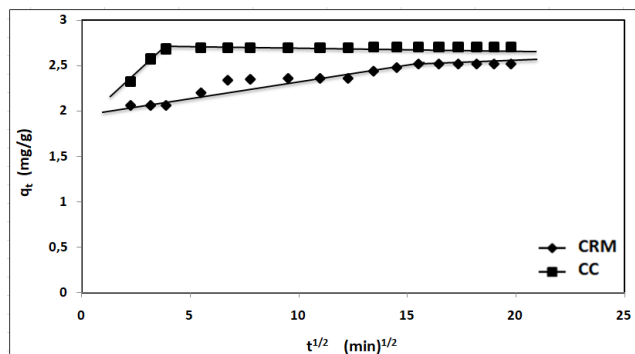
Figure 18. The plots of intraparticle diffusion model for MV adsorption onto CRM and CC.

With the help of these figures drawn on the basis of equations (4), (5) and (6), the kinetic constants have been calculated and the results are shown in Tables 2 and 3. As shown in Table 2, the R^2 values of the pseudo second order exceeded 0.99 for MV adsorption onto CRM and CC which were higher than those of pseudo first order, and the adsorption capacity at equilibrium values $q_{e,exp}$ were

closer with the theoretical calculated values $q_{e,cal}$ compared to the pseudo first order model. This indicated the applicability of the pseudo second order kinetic model to describe the adsorption process of MV onto CRM and CC. Figure 18 shows the intraparticle diffusion plots for adsorption of MV onto CRM and CC. As seen from this figure, the plots are not linear over the whole-time range, which indicates that more than one mode of sorption, is involved in the MV adsorption. These multiple linear plots indicating that intraparticle diffusion plays a significant role but is not the only rate limiting step and boundary layer control may be involved in the adsorption process. For CRM and CC, the adsorption process exhibits only two stages, being the first linear part attributed to intraparticle diffusion, and the second stage is the diffusion through smaller pores, which is followed by the establishment of equilibrium (Vaghetti *et al.*, 2009). The results showed that the adsorption process is complex and involves more than one mechanism. The K_d and C values calculated from the first region of the plots are given in Table 3.

Table 2. Kinetic parameters for MV adsorption onto CRM and CC.

Adsorbents	CRM	CC
$q_{e,exp}$ (mg/g)	2.520	2.700
Pseudo – first order		
$q_{e,cal}$ (mg/g)	0.599	0.128
k_1 (min^{-1})	0.012	0.024
R^2	0.725	0.413
Pseudo – second order		
$q_{e,cal}$ (mg/g)	2.513	2.710
k_2 (*g/mg.min*)	0.103	0.879
R^2	0.998	1

Table 3. Intraparticle diffusion model parameters for the adsorption of MV dye onto CRM and CC.

Adsorbents	CRM	CC
K_d(mg / g.min$^{1/2}$)	0.035	0.223
C (mg/g)	1.981	1.833
R^2	0.919	0.978

3.4. Isotherm modeling

Adsorption isotherm is important for the optimization of adsorbent used and also to describe the interaction between the adsorbate and adsorbent. For this purpose, three widely used isotherm models, Langmuir, Freundlich and Temkin, were employed to interpret the experimental data at 20°C using the optimal values of agitation speed, adsorbent dose and initial pH.

Langmuir Isotherm: A well – known linear expression for the Langmuir isotherm (Langmuir *et al.*, 1918) is represented as:

$$\frac{C_e}{q_e} = \frac{1}{q_m K_L} + \frac{1}{q_m} C_e \tag{7}$$

Where C_e is the equilibrium concentration (mg/ L), q_e is the amount of adsorbate adsorbed per unit mass of adsorbent at equilibrium (mg/g), q_m is the theoretical maximum adsorption capacity of adsorbate per unit mass

of adsorbent (mg/g), K_L is the Langmuir isotherm equilibrium constant related to the energy of adsorption (L/mg). The values of q_m and K_L can be determined from the slope and intercept of linear plot of $\frac{C_e}{q_e}$ versus C_e.

The results are presented in Figure 19.

Freundlich isotherm: The linear expression of the Freundlich equation is generally expressed as follows (Freundlich *et al.*, 1906):

$$\ln q_e = \ln K_F + \frac{1}{n} \ln C_e \tag{8}$$

Where K_F is the Freundlich adsorption constant related to adsorption capacity of the adsorbent (mg/g).(L/mg)$^{1/n}$ and $\frac{1}{n}$ is the adsorption intensity. The values of K_F and $\frac{1}{n}$ were calculated from the intercept and slope of the plot $\ln q_e$ versus $\ln C_e$ (Figure 20)

Temkin isotherm: The linear form of Temkin isotherm is expressed as (Temkin *et al.*, 1940):

$$\mathbf{q}_e = B_T ln\ K_T + B_T ln\ C_e \qquad (9)$$

Where B_T is the Temkin constant related to the heat of adsorption and K_T is the Temkin equilibrium binding constant (L/mg). The constant B_T and K_T can be determined by a plot of q_e versus lnC_e (Figure 21).

All the correlation coefficient R^2 values and the constants obtained from the three isotherm models are summarized in Table 4. The best fit isotherm model with the experimental data was chosen based on the highest R^2 value. In the Table 4, comparison of the R^2 values shows that the Langmuir isotherm fitted quite well with the experimental data with high R^2 values for CRM ($R^2 = 0.92$) and CC ($R^2 = 0.968$) at 20°C. The Langmuir model assumes that the adsorbate will only form one layer on the adsorbent's surface. Also, it shows that the Langmuir isotherm gave the maximum adsorption capacity of 9.804 mg/g and 62.5 mg/g for MV onto CRM and CC at 20°C, respectively. It can be seen from these results that the maximum adsorption capacity value of CC is higher than those of many adsorbents such as Mansonia wood sawdust (q_m = 22.1 mg/g) (Ofomaja *et al.*, 2008) and bagasse fly ash (q_m = 26.25 mg/g) (Mall *et al.*, 2006). Therefore, the char CC prepared in this study could be evaluated a promising biomass for especially dye adsorption studies. This can also be concluded from the Freundlich model fitting results shown in Table 4. The value of n for Freundlich isotherm was found to be larger than 1, indicating that MV is favorably adsorbed by CRM and CC at 20°C (Tunali *et al.*, 2006).

Table 4. Langmuir, Freundlich and Temkin isotherm constants for adsorption of MV onto CRM and CC at 20 °C.

		q_m (mg/g)	K_L (L/mg)	R^2
CRM	**Langmuir**	9.804	0.604	0.920
	Freundlich	n	K_F	R^2
		1.032	0.294	0,772
	Temkin	B_T	K_T (L/mg)	R^2
		2.213	6.642	0.815
CC	**Langmuir**	q_m (mg/g)	K_L (L/mg)	R^2
		62.500	0.254	0,968
	Freundlich	n	K_F	R^2
		2.833	14.865	0,960
	Temkin	B_T	K_T (L/mg)	R^2
		8.494	9.071	0,893

Table 5. Thermodynamic parameters of adsorption of MV onto CRM and CC

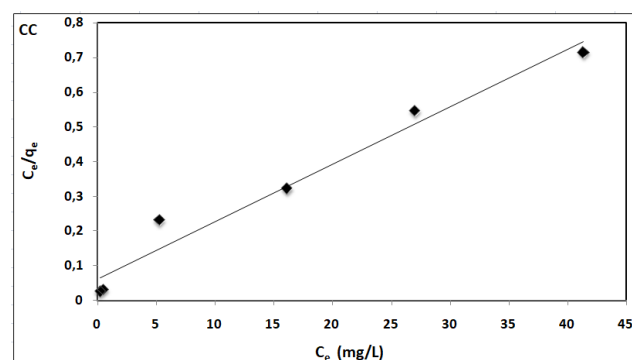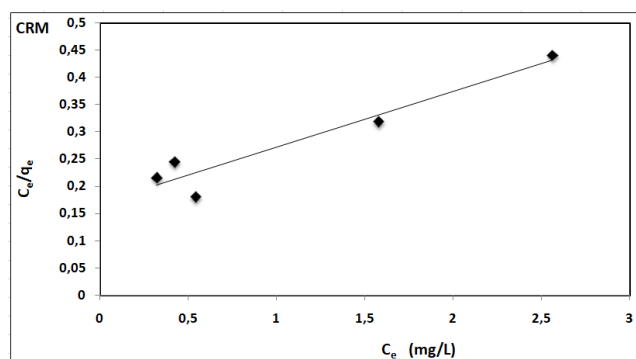| Adsorbents	ΔH° (kJ/mol)	ΔS° (J/mol.K)	T (K)	ΔG°(kJ/mol)	R^2
CRM	-35.017	-105.796	293.15	-4.003	0.958
			303.15	-2.945	
			313.15	-1.887	
CC	-32.952	-94.879	293.15	-5.138	0.957
			303.15	-4.189	
			313.15	-3.241	

Figure 19. Langmuir linear adsorption isotherms of MV onto CRM and CC at 20°C.
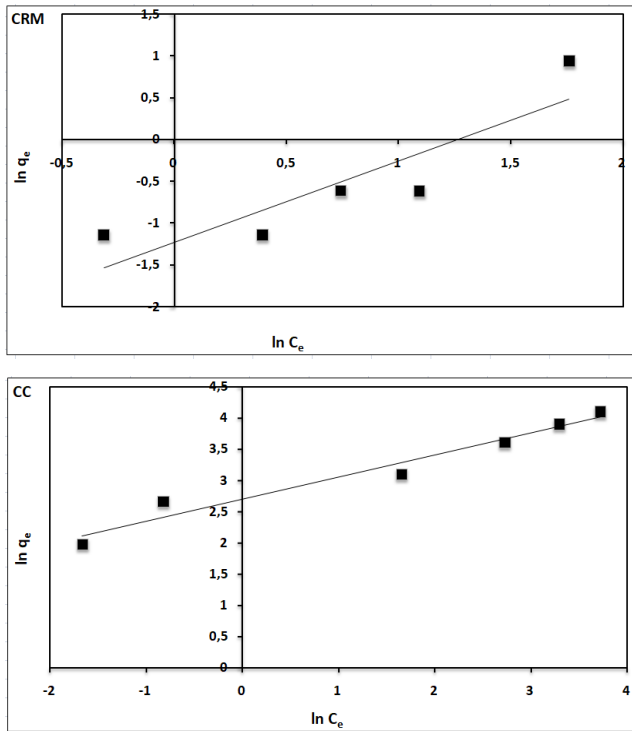
Figure 20. Freundlich linear adsorption isotherms of MV onto CRM and CC at 20°C.
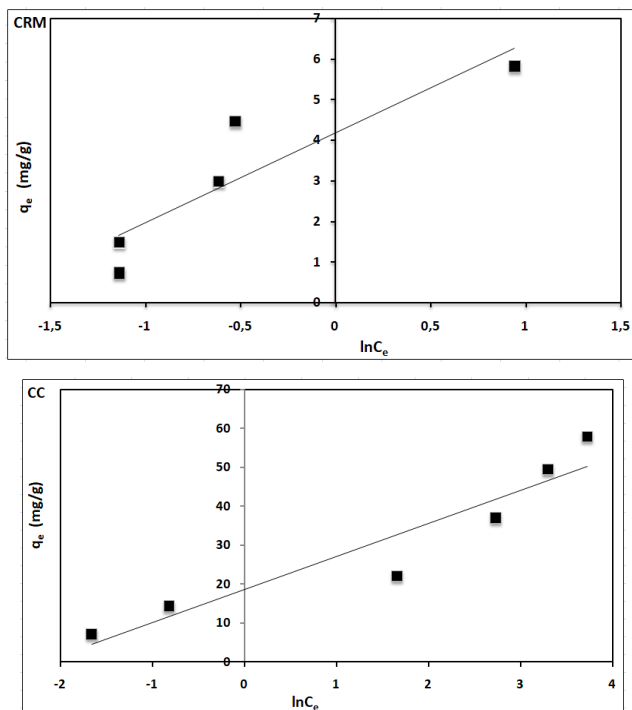

Figure 21. Temkin linear adsorption isotherms of MV onto CRM and CC at 20°C.

3.5. Thermodynamic Parameters

In order to describe thermodynamic behavior of the adsorption of MV onto CRM and CC, thermodynamic parameters including the change in free energy $\Delta G°$, enthalpy $\Delta H°$ and entropy $\Delta S°$ were calculated from following equations (Güzel *et al.*, 2015; Farhan *et al.*, 2012):

$$\Delta G° = -RT \, ln \, K_e \tag{10}$$

Where R is the universal gas constant (8.314 J/mol. K), T (K) is the temperature. The thermodynamic equilibrium constant K_e of the adsorption process is defined as:

$$K_e = \frac{C_{a\,ads}}{C_e} = \frac{C_0 - C_e}{C_e} \tag{11}$$

Where, $C_{a\,ads}$ is the mass of adsorbate adsorbed per liter of solution (mg/L), C_0 is the initial dye concentration (mg/L), and C_e is the equilibrium concentration of solution (mg/L). According to thermodynamics, the Gibb's free energy change $\Delta G°$ is also related to the enthalpy change $\Delta H°$ and entropy change $\Delta S°$ at constant temperature by:

$$\Delta G° = \Delta H° - T\Delta S° \tag{12}$$

Equations (10) and (12) can be written as:

$$\Delta G° = -RT \, ln \, K_e = \Delta H° - T\Delta S°$$

$$ln \, K_e = \frac{\Delta S°}{R} - \frac{\Delta H°}{R} \times \frac{1}{T} \tag{13}$$

According to the equation (13), the values of enthalpy change $\Delta H°$ and entropy change $\Delta S°$ were calculated from the slope and intercept of the plot of lnK_e versus $\frac{1}{T}$ (Figure 22). The calculated values of thermodynamic variables such as the Gibbs free energy $\Delta G°$, enthalpy $\Delta H°$ and entropy $\Delta S°$ for the adsorption of MV onto CRM and CC are reported in Table 5. Generally, the change of Gibbs free energy $\Delta G°$ for physisorption is between −20 and 0 kJ/mol, but chemisorption is in the range of −400 to −80 kJ/mol (Tunali *et al.*, 2006). The negative $\Delta G°$ values for CRM and CC at 20, 30 and 40 °C, are due to the fact that adsorption is a spontaneous physical process. The negative value of $\Delta H°$ for the two adsorbents indicates that the process is exothermic. Meanwhile, the negative value of $\Delta S°$ indicated a decrease in randomness within the system at the solid/solute interface during the adsorption of MV onto CRM and CC. This negative value of $\Delta S°$ suggests the formation of ordered activated complex. This behavior (negative values of $\Delta G°$, $\Delta H°$ and $\Delta S°$ and physisorption) was also observed by other researchers that employed adsorbents for removal of cationic dyes (Bonettoa *et al.*, 2015; Mahdavinia *et al.*, 2014; Manimekalai *et al.*, 2015)
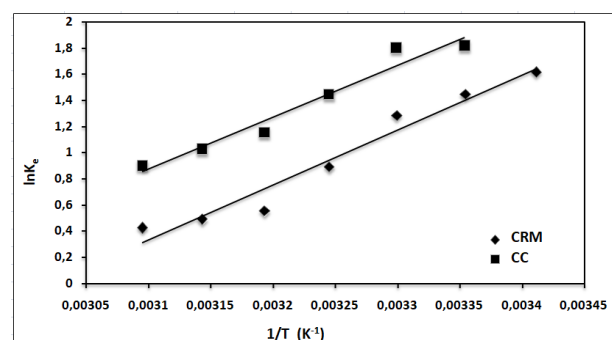

Figure 22. Plot of lnK_e versus $\frac{1}{T}$ for MV adsorption onto CRM and CC.

4. Conclusion

The results of this work can be summarized as follows:

1. FTIR spectrums and SEM micrographs of CRM and CC confirm the adsorption of MV onto these adsorbents.

2. CRM with particle size ≤ 0.08 – 0.125 mm shows a higher removal percentage (84.1% – 85%). The adsorption of MV was found to increase with increasing contact time for CRM and CC. The optimum agitation speed for MV removal was found to be 500 rpm for CRM and 300 for CC, with removal percentage 80.4% and 91% respectively. The maximum MV removal percentages were 87.6% and 89.9 % onto CRM and CC at the dosages 1 g and 0.05 g respectively. The pH significantly affected the adsorption percentage onto the two adsorbents. The optimum adsorption was found at pH = 8 for CRM (R= 87.5%) and at pH = 9 for CC (R= 89.8%). The optimal value of the temperature was 20°C for CRM (R=83.4%) and CC (R = 87%). As the ionic strength increased, the adsorption percentage increased from 80.4% to 100% for CRM and from 84.5% to 92.5% for CC. The adsorption capacity at equilibrium q_e increased with an increase in the initial MV concentrations.

3. The kinetic data were well described by the pseudo second order model with higher correlation coefficients and also the experimental $q_{e, exp}$ values agree with the calculated ones.

4. Equilibrium adsorption data were well fitted to the Langmuir isotherm model with higher correlation coefficients than the other models for CRM and CC at 20°C, showing maximum capacity of 62.5 mg/g onto CC and 9.804 mg/g onto CRM.

5. The calculated thermodynamic parameters show the spontaneous and exothermic natures of the adsorption process.

In view of these results, it can be concluded that the CRM and CC can be utilized as low-cost alternative adsorbents for the removal of cationic dyes from aqueous phase.

References

Ahmad M.A., Eusoff M.A., Adegoke K.A., and Bello O.S. (2021). Sequestration of methylene blue dye from aqueous solution using microwave assisted dragon fruit peel as adsorbent, *Environmental Technology & Innovation* 24, 101917.

Akinhanmi T.F., Ofudje E.A., Adeogun A.I., Aina P., and Joseph I.M. (2020). Orange peel as low-cost adsorbent in the elimination of Cd(II) ion: kinetics, isotherm, thermodynamic and optimization evaluations, *Bioresources and Bioprocessing*, **7**, 34.

Amin N.K. (2009). Removal of direct blue – 106 dye from aqueous solution using new activated carbons developed from pomegranate peel: adsorption equilibrium and kinetics, *Journal of Hazardous Materials*, **165**, 52–62.

Astuti W., and Maziyyah Fatin D. (2017). Adsorption of methyl violet dye by thermally modified *Ceiba pentandra* Sawdust, *Jurnal Bahan Alam Terbarukan,* **6** (2), 183–189.

Auta M., Darbis N., Din A., and Hameed B. (2013). Fixed – bed column adsorption of carbon dioxide by sodium hydroxide modified activated alumina, *Chemical Engineering Journal,* **233**, 80–87.

Behrami E., Xhaxhiu K., Dragusha B., Reka A., Andoni A., Hamiti X., and Drushku S. (2022). The removal of atrazine and benalaxyl by the fly ash released from Kosovo, a power plant, *International Journal of Analytical Chemistry*, **2022**, 1–10.

Bonettoa L.R., Ferrarini F., De Marcoa C., Crespoa J.S., Guéganb R., and Giovanelaa M. (2015). Removal of methyl violet 2B dye from aqueous solution using a magnetic composite as an adsorbent, *Journal of Water Process Engineering*, **6**, 11–20

Bouaouina K., Barras A., Bezzi N., Amin M.A., Szunerits S., and Boukherroub R. (2022). Adsorption-reduction of Cr(VI) onto unmodified and phytic acid-modified carob waste: Kinetic and isotherm modeling, *Chemosphere*, **4**, 134188.

Bounaas M., Bouguettoucha A., Derradji C., Gatica J.M., and Vidal H. (2021). Role of the wild carob as biosorbent and as precursor of a new high surface area activated carbon for the adsorption of methylene blue, *Arabian Journal for Science and Engineering*, **46**, 325–341.

Cengiz S., and Cavas L. (2010). A promising evaluation method for dead leaves of *Posidonia oceanica* (L.) in the adsorption of methyl violet, *Marine Biotechnology*, **12**, 728–36.

Ciolacu D., Ciolacu F., and Popa V.I. (2011). Amorphous cellulose – structure and characterization, *Cellulose Chemistry and Technology*, **45** (1-2), 13–21.

Dahri M.K., Kooh M.R.R., and Lim L.B.L. (2016). Adsorption of toxic methyl violet 2B dye from aqueous solution using *Artocarpus heterophyllus* (Jackfruit) seed as an adsorbent, *American Chemical Science Journal*, **15**, 1–12.

Daramy M.A., Kawada R., and Oba S. (2020). What is the threshold carbonization temperature for sustainable preservation of the good nitrogen supply ability of chicken manure? *Sustainability*, **3306**,1–19.

Deniz Çiftçi T., and İşlek Coşkun Y. (2020). Removal of Pb (II) from water using (Fe3O4/Ni/NixB) magnetic nanocomposites, carob (*Ceratonia siliqua*) or grape seeds (*Vitis vinifera*), *Journal of Water Chemistry & Technology*, **42**(3), 185–195.

Duan J., Liu R., Chen T., Zhang B., and Liu J. (2012). Halloysite nanotubes – Fe3O4 composite for removal of methyl violet from aqueous solutions, *Desalination,* **293**, 46–52.

Eba F., Gueu S., Mvongbote A.E., Ondo J.A., Yao B.K., Nlo J.N., and Biboutou R.K. (2010). Evaluation of the adsorption capacity of the natural clay from Bikougou (Gabon) to remove Mn (II) from aqueous solution, *International Journal of Engineering and Technology,* **2**, 5001–5016.

Elass K. Laachach A., Alaoui A., and Azzi M. (2011). Removal of methyl violet from aqueous solution using a stevensite rich clay from Morocco, *Applied Clay Science*, **54**, 90–96.

Eren E., Cubuk O., Ciftci H., Eren B., and Caglar B. (2010). Adsorption of basic dye from aqueous solutions by modified sepiolite: equilibrium, kinetics and thermodynamics study, *Desalination*, **252**, 88–96.

Eren V.S., Deo Mall I., and Srivastava V.C. (2007). Kinetic and equilibrium isotherm studies for the adsorptive removal of brilliant green dye from aqueous solution by rice husk ash, *Journal of Environmental Management*, **84**, 390–400.

Farnane A.M., Salem N.M., Ahmad A.L., and Awwad A.M. (2012). Kinetic, equilibrium and thermodynamic studies of the biosorption of heavy metals by *Ceratonia Siliqua* Bark, *American Journal of Chemistry*, **2**, 335–342.

Farnane M., Tounsadi H., Elmoubarki R., Mahjoubi F.Z., Elhalil A., Saqrane S., Abdennouri M., Qourzal S., and Barka N. (2017). Alkaline treated carob shells as sustainable biosorbent for clean recovery of heavy metals: Kinetics, equilibrium, ions interference and process optimization, *Ecological Engineering*, **101**, 9–20.

Freundlich H.M.F. (1906). Over the Adsorption in Solution, *Journal of Physical Chemistry*, **57**, 385–470.

Gallagher K.A., Healy M.G., and Allen S.J. (1997). Biosorption of synthetic dye and metal ions from aqueous effluents using fungal biomass, *Studies in Environmental Science*, **66**, 27–50.

Germplasm Resources Information Network (GRIN). (2017). "*Ceratonia siliqua*". Agricultural Research Service (ARS), United States Department of Agriculture (USDA).

Gezer B. (2018). Adsorption capacity for the removal of organic dye pollutants from wastewater using carob powder, *International Journal of Agriculture, Forestry and Life Science*, **2**, 1–14.

Guillén R. A., Lizama-Bahena C., Trevino-Quintanilla L.G., Barragan-Trinidad M., Bustos V., and Moeller-Chavez G. (2022). Peat as a potential biomass to remove azo dyes in packed biofilters, *Biomass*, **April**, 1-18.

Güzel F., Sayğili H., Sayğili G.A., and Koyuncu F. (2015). New low-cost nanoporous carbonaceous adsorbent developed from carob (*Ceratonia siliqua*) processing industry waste for the adsorption of anionic textile dye: Characterization, equilibrium and kinetic modeling, *Journal of Molecular Liquids.* **206**, 244–255.

Haber B. (2002). Carob fiber benefits and applications, *Cereal Foods World*, **47**, 365–369.

Hema M., and Martin Deva Prasath P. (2009). Adsorption of malachite green onto carbon prepared from *borassus bark*, *The Arabian Journal for Science and Engineering*, **34**, 31–42.

Jaikumar V., and Ramamurthi V. (2009). Effect of biosorption parameters kinetics isotherm and thermodynamics for acid green dye biosorption from aqueous solution by brewery waste, *International Journal Chemistry*, **1**, 2–12.

Kabra A.N., Khandare R.V., Waghmode T.R., and Govindwar S.P. (2012). Phytoremediation of textile effluent and mixture of structurally different dyes by *Glandularia pulchella* (Sweet) Tronc, *Chemosphere*, **87**, 265–272.

Karaoğlu M.H., Doğan M., and Alkan M. (2010). Kinetic analysis of reactive blue 221 adsorption on kaolinite, *Desalination*, **256**, 154–165.

Kim T.Y., Parks S.S., and Cho S.Y. (2012). Adsorption characteristics of reactive black 5 onto chitosan beads cross–linked with epichlorohydrin, *Journal of Industrial and Engineering Chemistry*, **18**, 1458–1464.

Kismir Y., and Aroguz A.Z. (2011). Adsorption characteristics of the hazardous dye brilliant green on Saklikent mud, *Chemical Engineering Journal*, **172**, 199–206.

Kumar P.S., Ramalingam S., Senthamarai C., Niranjanaa M., Vijayalakshmi P., and Sivanesan S. (2010). Adsorption of dye from aqueous solution by cashew nutshell: studies on equilibrium isotherm, kinetics and thermodynamics of interactions, *Desalination*, **261**, 52–60.

Lagergren S. (1898). About the theory of so – called adsorption of soluble substances, *Kungliga Svenska Vetenskapsakademiens*, Handlingar, **24**, 1–39.

Langmuir I. (1918). The adsorption of gases on plane surfaces of glass, mica and platinum, *Journal of the American Chemical Society*, **40**, 1361–1403.

Mahdavinia G.R., Massoudi A., Baghban A., and Shokri E. (2014). Study of adsorption of cationic dye on magnetic kappa – carrageenan/PVA nanocomposite hydrogels, *Journal of Environmental Chemical Engineering*, **2**, 1578–1587.

Mall I.D., Srivastava V.C., and Agarwal N.K. (2006). Removal of orange – G and methyl violet dyes by adsorption onto bagasse fly ash-kinetic study and equilibrium isotherm analyses, *Dyes Pigments*, **69**, 210–223.

Manimekalai T. K., Sivakumar N., and Periyasamy S. (2015). Real–world mixed plastics waste into activated carbon and its performance in adsorption of basic dye from textile effluent, *Digest Journal of Nanomaterials and Biostructures*, **10** (3), 985–1001.

Ofomaja A.E., and Ho Y.S. (2008). Effect of temperatures and pH on methyl violet biosorption by Mansonia wood sawdust, *Bioresources Technology*, **99**, 5411–5417.

Oladoja N.A., and Akinlabi A.K. (2009). Congo red biosorption on palm kernel seed coat, *Industrial and Engineering Chemistry Research*, **48**, 6188–6196.

Patil S., Deshmukh V., Renukdas S., and Patel N. (2011). Kinetics of adsorption of crystal violet from aqueous solutions using different natural materials, *International Journal of Environmental Science*, **1**, 1116–1134.

Ramírez-Montoya A.L., Hernández – Montoya V., and Montes – Morán M.A. (2014). Optimizing the preparation of carbonaceous adsorbents for the selective removal of textile dyes by using Taguchi methodology, *Journal of Analytical and Applied Pyrolysis*, **109**,9–20.

Ramutshatsha – Makhwedzha D., Mbaya R., Mavhungu M.L. (2022). Application of activated carbon banana peel coated with Al_2O_3 – Chitosan for the adsorptive removal of lead and cadmium from wastewater, *Materials*, **15** (3), 860.

Sabnis R.W. (2010). Handbook of biological dyes and stains: Synthesis and industrial applications. Hoboken, New Jersey: John Wiley and Sons.

Salman M., Athar M., Shafique U., Rehman R., Ameer S., Ali S.Z., and Azeem M. (2012). Removal of formaldehyde from aqueous solution by adsorption on kaolin and bentonite: a comparative study, *Turkish Journal of Engineering and Environmental Sciences*, **36**, 263–270.

Santhi T., and Manonmani S. (2009). Removal of methylene blue from aqueous solution by bioadsorption onto *Ricinus communis* epicarp activated carbon, *Chemical Engineering Research Bulletin*, **13**, 1–5.

Sayğılı H., and Güzel F. (2018). Uptake of anionic and cationic dyes by highly effective porous carbon adsorber based on industrial processing residues, *Journal Separation Science and Technology*, **53**, 1465–1475.

Tanada S., Kita T., Boki K., Tamura T., and Murai Y., (1980). Mechanism of adsorption of methylene blue on magnesium silicate. *Chemical and Pharmaceutical Bulletin*, **28**, 2503–2506.

Temkin M.J., and Pyzhev V. (1940). Kinetics of ammonia synthesis on promoted iron catalysts, *Acta physicochimica USSR*, **12**, 217–222.

Treybal R. E. (1981). Mass Transfer Operations, 3rd Edn, McGraw–Hill, New York.

Tunali S., Özcan A.S., Özcan A., and Gedikbey T. (2006). Kinetics and equilibrium studies for the adsorption of acid red 57 from aqueous solutions onto calcined – alunite, *Journal of Hazardous Materials*, **135**, 141–148.

Vaghetti J.C.P., Lima E.C., Royer B., Da Cunha B.M., Cardoso N.F., Brasil J.L., and Dias S.L.P. (2009). Pecan nutshell as biosorbent to remove Cu(II), Mn(II) and Pb(II) from

aqueous solutions, *Journal of Hazardous Materials*, **162**, 270–280.

Weber W.J., and Morris J.C. (1963). Kinetics of adsorption on carbon from solutions, *Journal of the Sanitary Engineering Division,* **89**, 31–60.

Xu R.K., Xiao S.C., Yuan J.H., and Zhao A.Z. (2011). Adsorption of methyl violet from aqueous solutions by the biochars derived from crop residues, *Bioresource Technology,* **102**, 10293–10298.

Yao Y., He B., Xu F. and Chen X. (2011). Equilibrium and kinetic studies of methyl orange adsorption on multiwalled carbon nanotubes, *Chemical Engineering Journal*, **170**, 82–89.

Yu J., Zhu Z., Zhang H., Di G., Qiu Y., Yin D., and Wang S. (2020). Hydrochars from pinewood for adsorption and nonradical catalysis of bisphenols, *Journal of Hazardous Materials*, **385**, 121548.